Citation
Liu, Y. and Paskevicius, M. and Wang, H. and Parkinson, G. and Wei, J. and Asif Akhtar, M. and Li, C.Z. 2021. Insights into the mechanism of tar reforming using biochar as a catalyst. Fuel. 296. http://doi.org/10.1016/j.fuel.2021.120672

Insights into the mechanism of tar reforming using biochar as a catalyst

Yurong Liu[1*], Mark Paskevicius[1], Hongqi Wang[1], Gordon Parkinson[1], Juntao Wei[1,2], Muhammad Asif Akhtar[1], Chun-Zhu Li[1,3]

1: Fuels and Energy Technology Institute, Curtin University, GPO Box U1987, Perth, WA 6845, Australia

2: Joint International Research Laboratory of Biomass Energy and Materials, College of Materials Science and Engineering, Nanjing Forestry University, Nanjing 210037, China

3: Department of Chemical Engineering, The University of Western Australia, 35 Stirling Highway, Perth, WA 6009, Australia

[*] *Corresponding author: yurong.liu@postgrad.curtin.edu.au*

Abstract

Biochar is an efficient catalyst for tar removal from syngas during biomass gasification. The aim of this research is to investigate the mechanism of tar reforming using biochar as a catalyst. A series of *in situ* steam tar reforming experiments were carried out using a two-stage fluidized-bed/fixed-bed reactor at 800 °C. Mallee wood biochar (106–250 µm) was activated in 15 vol. % H_2O balanced with Ar for different times (0–50 min) and then used as a catalyst for tar reforming. The on-line gas composition, light tar composition and the pore structure of biochar were analysed using mass spectrometer (MS), GC-MS and synchrotron small angle X-ray scattering (SAXS) respectively. An increased ratio of H_2/CO was observed after reforming with biochar compared to reforming without biochar. The destruction of light tar compounds, especially the non-oxygen-containing compounds, was significantly enhanced when activated biochars were used. Steam activation increased the specific surface area (SSA), micro- and mesopore volumes in biochar while the values stayed almost unchanged during tar reforming. Results indicate that the micro- and mesopores in

biochar promote the diffusion of both small and large tar molecules into the internal surface of biochar. However, the catalytic activity of biochar for tar reforming mainly depends on the content of O-containing functional groups in biochar. The O-containing functional groups facilitate the dissociation of tar molecules to form tar radicals, giving rise to the enhanced tar removal efficiency. Moreover, the formation of tar radicals over O-containing functional groups appears as the rate-limiting step in the process of catalytic reforming of tar over biochar catalysts.

Keywords: Steam tar reforming, biochar catalyst, specific surface area, pore volume, mechanism

1. Introduction

Biomass gasification is considered to be one of the most promising technologies to expand the contribution of biomass to the world's renewable energy supply [1,2]. However, tar formation is practically unavoidable during gasification, and the removal of tar from syngas is one of the major technical barriers that limits the commercialization of gasification technologies [3]. Extensive gas cleaning is required before the product gas is used for electricity generation, as well as for the synthesis of chemicals and transportation fuels.

Amongst the various methods used for tar removal, catalytic steam reforming appears to be the most promising technique [4,5]. The use of biochar as a catalyst is particularly attractive due to its high catalytic efficiency and low cost [6–9]. In addition, the energy value of spent biochar can be recovered simply by further gasifying or burning. Understanding the reaction mechanism of tar reforming over biochar is critical for

optimizing the catalytic performance of biochar, as well as for the development of gasification technologies.

It has been proposed that the two main reaction pathways of tar during steam reforming are homogeneous and heterogeneous reforming [10,11]. However, due to the complex composition of tar as well as the complex properties of biochar, the reforming mechanism of tar using biochar as a catalyst has not yet been fully elucidated. Particularly, little is known about the interactions between tar molecules and the active sites in biochar in the heterogeneous reforming process. Great efforts [10,12–19] have been made to study the factors that influence the catalytic activities of tar removal over biochar catalysts. Apart from the experimental conditions such as temperature [17,20] and gasifying agents [12,16], the physicochemical properties of biochar, particularly the porous structure (large specific surface area) [14,21], the surface chemistry [6,12,13], as well as the inherent alkali and alkaline earth metallic (AAEM) species [15] are considered to be the main factors that affect the catalytic activity of biochar. However, the results [14,21,22] are not consistent regarding the relative importance of the micro- and mesopores in biochar. The exact role of the active sites in biochar for heterogeneous tar reforming is also ambiguous. Above all, it remains unclear which step involved in the heterogeneous reforming process is the rate-determining step. Therefore, further studies are needed to fully understand the mechanism of tar reforming over biochar catalysts.

In our previous studies [12,13], the O-containing functional groups, especially the aromatic C-O structures, in biochar have been recognized to be a key factor influencing its catalytic activity. It is also critical to investigate the evolution of the pore structure of biochar during tar reforming in order to identify the key property of biochar that limits its

catalytic activity for tar reforming. Moreover, the distribution of product gas and the formation rate of each gas is directly related to the reaction types and reaction rate. The behaviour of various tar molecules during tar reforming would be also differ with their own structural features and activities. For example, some tar compounds would be preferentially reformed over biochar, whereas some may mainly be destructed in the gas phase [16]. Therefore, a comprehensive analysis of tar composition and the product gas composition is also essential for a better understanding the reaction mechanism of tar reforming.

For these reasons, following our previous study [13], we investigate the evolution in the pore structure of biochar catalysts as well as the gas composition during reforming in this work. Moreover, the tar composition after steam reforming was also analysed with the aim to identify the main tar compounds that are preferentially destructed over biochar surface. In the end, a reforming mechanism is proposed, taking into consideration the interactions between O-containing functional groups and tar components. The possible deactivation mechanism of biochar catalyst during steam tar reforming is also considered. Our results would provide critical information on identifying the decisive factor influencing the catalytic activity of biochar, as well as on the understanding of the mechanism of tar destruction over biochar catalysts.

2. Experimental

2.1. *In situ* steam reforming of tar using biochar as a catalyst

Steam tar reforming experiments were carried out using a three-frit two-stage fluidised-bed/fixed bed quartz reactor [23,24], as shown in Fig. 1. The experimental conditions (800 °C, 15 vol. % H_2O mixed with Ar), biochar (106–250 μm) and bio-oil samples

94 used in this study were the same as those in our previous work [13]. Briefly, biochar
95 samples were preloaded on the middle frit and *in-situ* activated in a 15 vol. % H_2O mixed
96 with Ar before acting as a catalyst. After the activation time (0 - 50 min) was reached, bio-oil
97 was injected into the reactor at a rate of 0.20 ml min^{-1}. Tar was generated immediately
98 when the bio-oil reached the reaction zone at 800 °C. The generated tar was mixed with
99 steam before passing through the biochar bed and going through catalytic steam reforming.
100 When the required time was reached, the experiments were terminated by stopping the
101 feeding of bio-oil and steam. The reactor was then lifted out of the furnace and cooled
102 down under argon flow. It should be noted that the experimental design results in the *in-*
103 *situ* formation of tar from bio-oil in parallel with reforming reactions and biochar
104 gasification. Therefore, the outlet gas composition and quantity is a product of all three
105 simultaneous phenomena.

106 The same method in our previous studies [25,26] was used to collect tar samples
107 after reforming. Briefly, the reactor outlet was connected to three condensation traps filled
108 with a mixture of HPLC-grade chloroform and methanol (4:1 by vol). Tar in the outlet stream
109 was then condensed in the mixture and collected for further analysis.

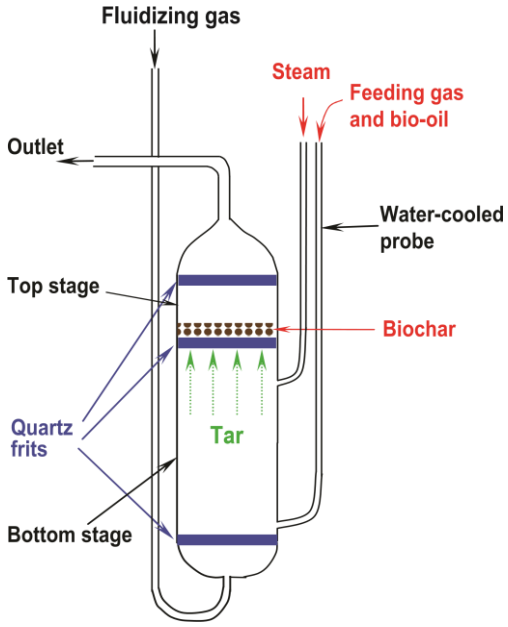

Fig. 1. A schematic diagram of the three-frit fluidized-bed/fixed-bed quartz reactor (modified from Ref. [23] with permission from Elsevier).

2.2. Characterisation of reforming products

After tar condensation and gas cooling, the outlet gas stream was connected to a QMS Prisma™ 200 mass spectrometer (MS) in order to monitor the real-time gas composition [27]. The MS was calibrated using a standard gas mixture (ISO Guide 34 accredited). As stated in our previous work [27], the CO signal was deconvoluted by subtracting the contribution of CO_2 at m/z = 28 as the mass fragment of CO_2 at m/z = 28 overlaps with CO signal. The molar/volume ratios of H_2, CO, CO_2, and CH_4 were calculated respectively afterwards.

Tar samples from the outlet stream were analysed using an Agilent GC–MS (a 6890 series GC plus a 5973 MS detector) with helium as the carrier gas. Detailed parameters of the measurement can be found elsewhere [28,29]. The detected compounds corresponding to each GC peak were identified based on the standard spectra of compounds in the

National Institute of Standards and Technology (NIST) library and/or the spectra of known species injected. The relative yield of each compound (*X*) was calculated by multiplying the peak area by the ratio of the amount of total tar solution collected and bio-oil injected (Eq. **Error! Reference source not found.**). Therefore, the relative yield of each compound was based on per g of bio-oil.

$$Relative\ yield\ of\ tar\ compound\ X\ = \frac{mass\ of\ total\ tar\ solution}{mass\ of\ bio{-}oil\ fed}\ integrated\ peak\ area\ of\ compound\ X \quad (1)$$

The porosity of biochar was characterised using Small Angle X-ray Scattering (SAXS) with a Pilatus 1-M detector at the Australian Synchrotron in Melbourne [30]. The procedures of measurement and data processing were detailed included in our previous studies [31,32]. Briefly, the measurements were conducted at two camera lengths (3343 mm and 959 mm) to achieve a wide *q* (*q* is the scattering vector $q = (4\pi/\lambda)\sin(\theta/2)$, λ (λ = 1.03 Å^{-1}) and θ are the wavelength and scattering angle) range from 0.005 to 1.5 Å^{-1}, respectively, which are appropriate for an approximate pore diameter ranging from 4 to 1250 Å. The SAXS intensities on absolute scale [33,34] were further processed with the unified model [35] in Irena described by Ilavsky et al [36] to obtain the specific surface area (SSA) and pore size distribution of biochar samples.

3. Results and discussion

3.1. Evolution in the gas composition

Before analysis, it should be noted that the outlet gas composition is the combined result of both tar reforming and the simultaneous gasification of biochar. The gas composition after 30 min of steam reforming with, and without, biochar is given as an

example to study the effect of the biochar catalyst on the gas composition, as shown in **Error! Reference source not found.**. Compared with reforming without biochar, the H_2 content greatly increased when reforming with biochar. The content of CO_2 also increased, whilst the content of CO and CH_4 decreased after using biochar as a catalyst. As such, the ratio of H_2/CO increased after reforming with biochar. It seems that the formation rate of H_2 was increased in the presence of biochar. This could be due to the enhanced catalyst (biochar)-gas (tar molecules) reactions, leading to the increased production of H_2.

Table 1. Product gas composition after steam reforming for 30 min with and/or without biochar.

Experiment conditions	Molar gas composition[a]				
	CO	CO_2	H_2	CH_4	H_2/CO molar ratio
Bio-oil only	62%	14%	4%	21%	0.07
Biochar only	37%	30%	20%	13%	0.55
Reforming with 0A biochar	38%	26%	22%	14%	0.58
Reforming with 10A biochar	35%	31%	22%	12%	0.63
Reforming with 20A biochar	33%	32%	23%	12%	0.70
Reforming with 30A biochar	30%	38%	21%	11%	0.70
Reforming with 40A biochar	29%	37%	25%	9%	0.80
Reforming with 50A biochar	29%	32%	28%	11%	0.83

Note: [a] dry basis; 0-50A biochar represent the biochar that was activated by steam for 0-50 min.

3.2. Evolution of light tar composition

Tar is a complex mixture of a large number of single aromatics (1 benzene ring), polycyclic aromatic hydrocarbon (PAH) compounds, along with other heterocyclic compounds such as O-containing tar compounds. Our previous study [13] investigated the evolution of relatively large PAH compounds in tar using UV-fluorescence spectroscopy. To obtain a more comprehensive understanding of the transformation and conversion of tar during steam reforming using biochar as a catalyst, we used GC-MS to investigate the evolution of light tar composition in the present study. It should be pointed out that GC-MS

has limitations in detecting tar with high molecular mass and highly polar compounds, thus only the relatively light tar compounds can be detected.

Fig. 2 and Fig. 3 show the GC-MS total ion chromatograms of tar samples after steam reforming with/without biochar with some relevant tar compounds marked. The peak height can roughly represent the content of the corresponding compound. It should be kept in mind that, in the process of tar reforming, some tar molecules such as phenol, indene and styrene can be formed from the breakdown of larger tar molecules. Therefore, the GC-MS detected tar compounds are the net results of their reforming/removal and formation. Fig. 2 compares the effect of steam activation time of biochar on the light tar composition. After steam reforming for 30 min, there is a clear trend when reforming with biochar that has been activated for different times, where the more activated biochar results in lower yields of these tar compounds. That is to say, longer biochar activation enhances the reforming/removal of light tar compounds. The light tar compounds were nearly completely reformed/removed after reforming for 10 - 30 min with biochar activated for 40 min in Fig. 3. However, peaks of styrene and naphthalene appear when the reforming time is increased to 50 min, as shown in Fig. 3c. This means that the activity of biochar on the reforming of light tar compounds decreased when the reforming time extended to 50 min. In our previous work [13], similar trend on the tar yield and the yield of relatively large aromatic ring system was observed. Thus, steam activation can enhance the catalytic activity of biochar on both the destruction of relatively large aromatic ring systems [13] and the removal of light tar compounds. Moreover, the catalytic activity of biochar decreases over the course of tar reforming [13]. The reduced catalytic activity of biochar at longer reforming time (e.g. 50 min) resulted in lower reforming rate of light tar compounds

detected by GC-MS compared to the rate of their formation. As such, increase in the contents of light tar compounds was observed here.

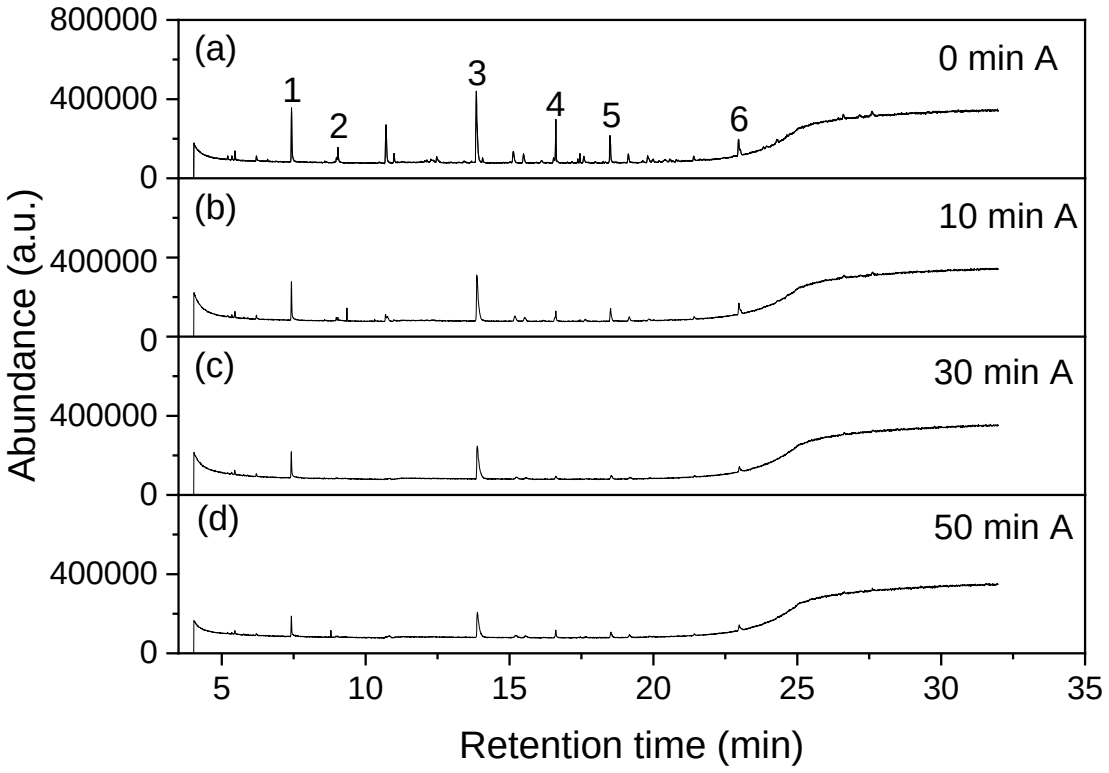

Fig. 2. GC–MS total ion chromatograms of the tars after reforming for 30 min (30 min R) with biochar activated for (a) 0 min, (b) 10 min, (c) 30 min and (d) 50 min. Note: A represents for activation; peak 1-styrene, peak 2-phenylacetylene, peak 3-naphthalene, peak 4-phenol, peak 5-acenaphthylene, peak 6-phenanthrene.

Studies [6,16,37] have found that the structure of tar molecules (aromatic ring sizes, functional groups, etc.) can affect its reactivity during reforming. For example, the aromatics with substituted groups or O-containing groups were reformed/removed relatively easily [16]. For this reason, the major light tar compounds detected by GC-MS were classified and

categorized into five component groups based on the structural features of tar compounds in this study, as shown in **Error! Reference source not found.**.

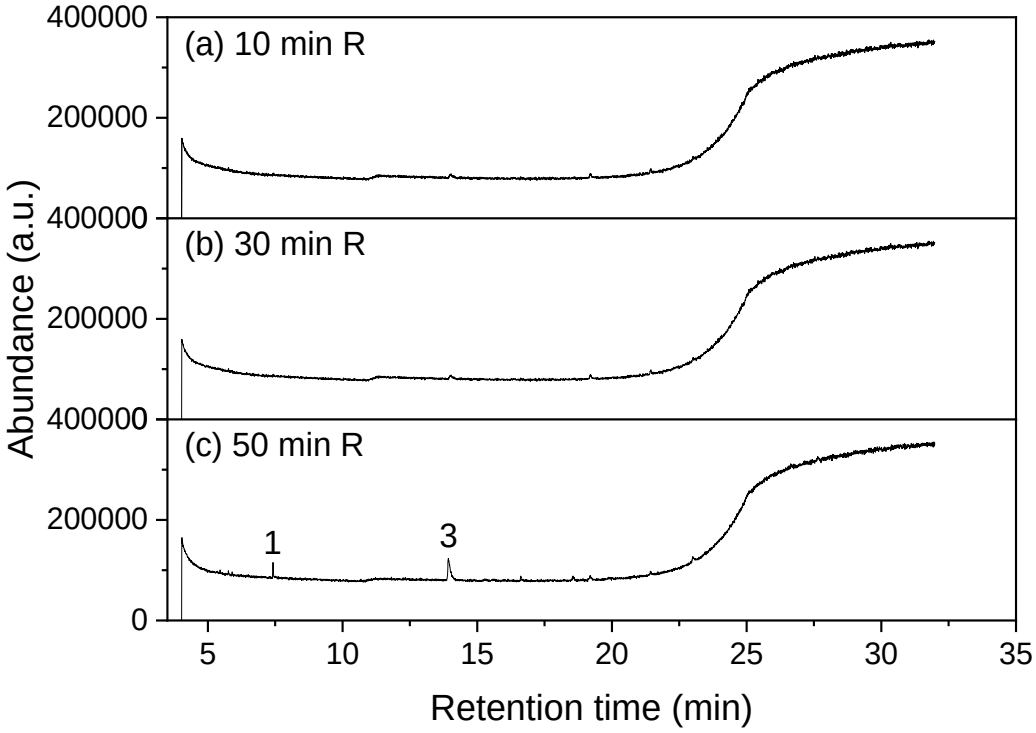

Fig. 3. GC–MS total ion chromatograms of the tars after reforming for (a) 10 min, (b) 30 min and (c) 50 min with biochar activated for 40 min (40 min A). Note: R for reforming; peak 1-styrene, peak 3-naphthalene.

Table 2. Classification of light tar compounds based on their structural features.

Group number	Compound groups	Compounds
1	naphthalene	naphthalene
2	phenanthrene	phenanthrene
3	aromatics (1-3 benzene rings) with penta-cycled ring or substituted groups	styrene, phenylacetylene, acenaphthylene, fluorene, indene, 1-methyl naphthalene, 2-methyl naphthalene
4	O-containing compounds	phenol, 3,4,5-trimethoxybenzaldehyde, dibenzofuran, benzofuran

The relative yield of different component groups in tars obtained from steam reforming with or without biochar are displayed in Fig. 4. The relative yields are presented

on the basis of per g of bio-oil. For all the tar samples from steam reforming, with or without biochar, the relative yields of naphthalene, and aromatics with penta-cycled ring or substituted groups, were much higher than those of phenanthrene or O-containing tar compounds. This has again indicated that the reactivity of tar molecules depends on their structural features. The aromatics with larger rings or O-containing groups were easier to be reformed/removed than smaller hydrocarbon aromatics [6,37,38].

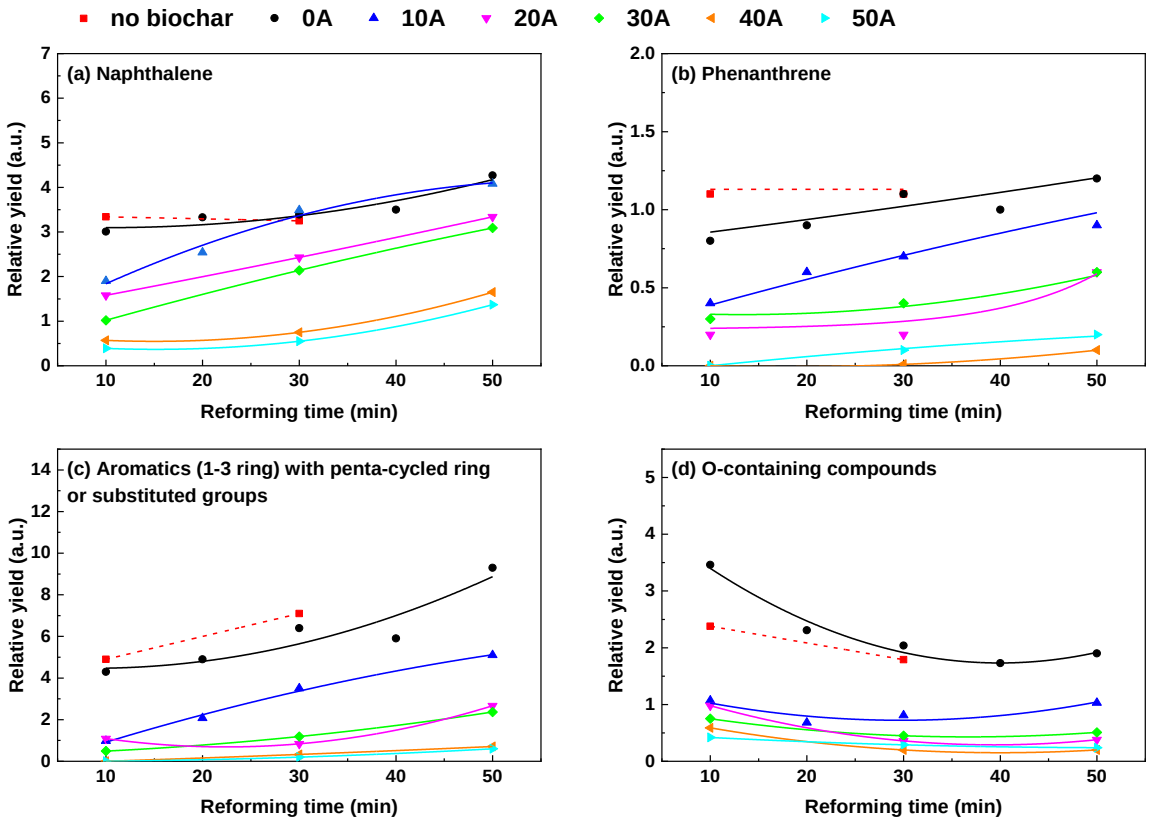

Fig. 4. Relative yield of the classified component groups from GC-MS: (a) naphthalene, (b) phenanthrene, (c) aromatics (1-3 benzene rings) with penta-cycled ring or substituted groups, (d) O-containing tar compounds. Note: 0-50A represents for 0-50 min activation.

The relative yield of light tar compounds all clearly decrease after reforming with activated biochars compared to reforming with raw biochar (0A) and/or without biochar (no

biochar). The longer the activation time of biochar, the lower the yield of non-oxygen-containing compounds (Fig. 4 a, b and c), with the same reforming time. Additionally, the yield of these compounds increased as a function of the reforming time. The results show that the activation of biochar has enhanced the removal of light tar compounds. Particularly, the decrease of light aromatics with penta-cycled ring or substituted groups (Fig. 4 c) was greater than other component groups such as naphthalene when using biochar activated for longer times. On the contrary, the variation in the activation time of biochar showed little effect on the reduction of the O-containing tar compounds (Fig. 4 d). Moreover, the yield of O-containing tar compounds almost stabilised at the same level as the reforming proceeded.

The trends of non-oxygen-containing groups illustrated by GC-MS are similar to that of the relatively large aromatic ring systems illustrated by UV-fluorescence spectroscopy in our previous study [13]. It was found that the yield of relatively large aromatic ring systems decreased when the activation time of biochar increased. The extension of reforming time led to a reduction in the yield of the relatively large aromatic ring systems. It was also confirmed that the steam activation of biochar greatly enhances its catalytic activity by increasing the content of O-containing functional groups. Besides, the catalytic activity of biochar reduces with increasing reforming time, with a decreasing content of O-containing functional groups in biochar. It seems that the catalytic activities of biochar in reforming light non-oxygen-containing tar compounds are also closely related to the content of O-containing functional groups in biochar. Whereas, the destruction of O-containing tar compounds is not greatly affected by the reduction in the O-containing functional groups of biochar.

The observations from UV-fluorescence spectroscopy [13] and GC-MS imply that the O-containing functional groups in biochar could be the main active sites for the reforming of large aromatic systems and light non-oxygen-containing tar compounds. In contrast, there could be other types of active sites in biochar on which the breakdown of O-containing tar compounds mainly take place. As such, the breakdown of O-containing tar compounds is not significantly improved with the increase of the O-containing functional groups in biochar, which result from longer activation times. Moreover, the active sites for O-containing tar compounds seem to show no sign of deactivation with the extension of reforming time (Fig. 4 d). One possible explanation is that these O-containing tar compounds are reformed mainly through conversion into gases rather than coke formation by condensation over biochar. Also it's possible that O-containing tar compounds are mainly adsorbed and reformed over other active sites (such as carbon) instead of O-containing functional groups in biochar.

3.3. Evolution in the pore structure of biochar catalysts

It has been suggested that that the pore structure of a porous catalyst is an important factor influencing its catalytic activity [39]. Therefore, it is necessary to study the changes in pore structure of biochar during steam activation and tar reforming.

Fig. 5 shows changes in the specific surface area (SSA), micropore volume (pore width < 2 nm) and mesopore volume (2 nm < pore width < 50 nm) of biochar during the steam activation and/or tar reforming processes. During activation/gasification (no bio-oil, dashed line in Fig. 5), the SSA (Fig. 5) of biochar increases with increasing activation time and reaches a maximum in 40 min before decreasing when the activation was prolonged to 50 min. The micropore volume (Fig. 5 b) and mesopore volume (Fig. 5 c) also show an

increasing trend at the early stage of activation before reaching a limiting size. The increased SSA, micro- and mesopore volumes are the result of carbon removal by steam activation/gasification of biochar, generating new pores, especially micropores [40,41]. The decreased SSA and micropore volume at the late stage of activation/gasification are attributed to the enlargement of micropores to mesopores and mesopores to macropores (pore width > 50 nm), meaning that fewer micro- and mesopores are left after a certain conversion level [40].

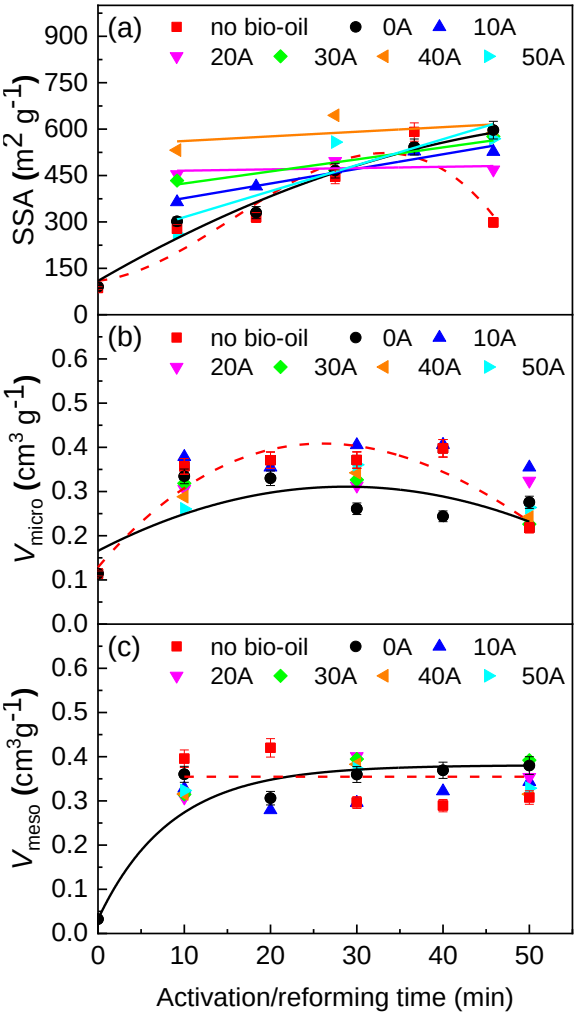

Fig. 5. Evolution of (a) SSA, (b) micropore volume (V_{micro}) and (c) mesopore volume (V_{meso}) of biochar during steam activation (dashed line) and reforming (solid line and data points) from

286 SAXS data. Note: 0-50A represents for 0-50 min activation, the dotted and plain lines are
287 referred to 0A.

288 The pores developed during activation could enhance the diffusion of tar molecules
289 to the internal catalytically active sites (e.g. O-containing functional groups), improving the
290 efficiency of tar destruction. It is also reasonable to believe that both the micro- and
291 mesopores in biochar are important in providing channels for the diffusion of the small and
292 large tar molecules considering that big tar molecules couldn't diffuse into micropores.
293 Moreover, as stated above, an abundance of O-containing functional groups were found to
294 be produced during steam activation of biochar previously [12,13]. The simultaneous
295 generation of O-containing functional groups and pores in biochar during steam activation
296 suggests that these O-containing functional groups are likely to distributed in the newly
297 created pores.

298 For the raw biochar that went through tar reforming (black solid line, 0A), the
299 development of increased SSA and pore volume with increasing time is analogous to that in
300 biochar that only underwent gasification (red dash line), where the values of SSA and pore
301 volumes are similar between the two cases. The presence of tar seems to have little effect
302 on the development of the pore structure in raw biochar. In the cases of activated biochars
303 (0-50A), the SSA and pore volumes stayed similar to one another and almost unchanged in
304 the process of tar reforming. This indicates that a high surface area and pore volume of
305 biochar does not always lead to a high efficiency of tar removal, which is quite dependent
306 on the activation time (Fig. 4). Furthermore, a good trend between the content of O-
307 containing functional groups in biochar and its catalytic activity for tar reforming was
308 observed previously [13]. When the O-containing functional groups dramatically reduce

309 with increasing reforming time [13], regardless of the surface area and pore volumes
310 observed here, the overall catalytic activity of the biochar decreases. The results suggest
311 that the O-containing functional groups play a more important role than surface
312 morphology in influencing the catalytic activity of biochar for tar reforming. It can also be
313 inferred that, under the experimental conditions in this work, the access and diffusion of tar
314 molecules through pores is not a key step in determining the efficiency of tar removal over
315 biochar. Our results disagree with some previous studies [14,21], in which they reported
316 that the specific surface area is the crucial factor determining the catalytic activity of biochar.
317 Therefore, focus should be directed towards optimising the O-containing functional groups
318 when producing a highly active biochar catalyst.

319 ### 3.4. Mechanism of tar reforming over biochar catalyst

320

321 Based on the above discussion, the following mechanism of tar reforming over
322 biochar is proposed. As illustrated in Fig. 6, the main steps involved in the reforming process
323 include the diffusion of tar molecules to internal catalytically active sites followed by the
324 adsorption and decomposition of tar molecules (C_nH_m) over active sites. The O-containing
325 functional groups in biochar would act as primary active sites, especially for the reforming of
326 relatively large aromatic ring systems and non-oxygen-containing tar compounds. The
327 overall efficiency of this reforming process is related to the pore structure and the content
328 of O-containing functional groups of biochar [13], with the latter being the dominant factor.
329 The small and large tar molecules firstly diffuse into the internal surface of biochar through
330 the micro- and mesopores in biochar.

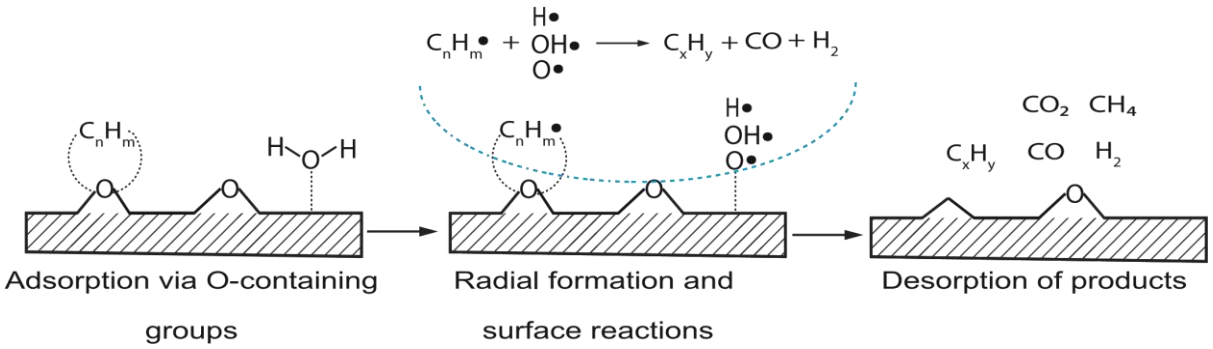

Fig. 6. Simplified mechanism of tar reforming via O-containing functional groups on biochar surface.

The tar molecules are then adsorbed on biochar surface via O-containing functional groups and dissociated into radicals. The formation of radicals is most likely to be the step in the mechanism that determines the reaction rate [3]. The presence of O-containing functional groups in biochar would facilitate the destabilisation of tar compounds, making them extremely active and easy to break into radicals. The breakdown of tar molecules is also associated with the structure of tar itself, where various tar structures would have different activation energies. The aromatics with more fused rings or penta-cycled rings/substituted groups tend to breakdown more easily as they are relatively active. In parallel to tar adsorption, H_2O present in the atmosphere is also adsorbed and dissociated on biochar, forming active radicals such as H, OH, and O, which could also react with each other.

The radicals from tar dissociation can react with the active radicals from H_2O to also form some small tar molecules (C_xH_y), as well as gases including CO and H_2, leading to the reforming/removal of tar compounds. Generated tar radicals could also react with each other to form larger tar molecules through polymerization and ultimately form coke. The presented H_2 in the system could also react with the tar radicals to form a stable tar

molecule and a hydrogen radical. As a result, a certain concentration of small and stable PAHs (polycyclic aromatic hydrocarbons) such as naphthalene is observed. Therefore, the final tar composition and the gas product distribution of tar reforming is the net result of all these parallel reactions that take place simultaneously in the reforming process.

As the complex reforming reaction proceeds, deactivation of a biochar catalyst will occur with the reduction of the O-containing functional groups. The binding between tar molecules and O-containing functional groups in biochar could also cause the O-containing functional groups to be decomposed with oxygen atoms being released from the biochar surface. Due to the lack of sufficient active sites at the late stage of reforming, the formation rate of tar radicals is significantly reduced, causing a decrease in the efficiency of tar removal. The mass loss of biochar caused by continuous gasification can lead to the reduction in catalytic efficiency of biochar catalyst as well.

4. Conclusions

Mallee wood biochar was activated *in situ* by steam and then used as a catalyst for steam tar reforming at 800 °C. The gas composition, light tar composition, as well as the SSA and pore volume of biochar were comprehensively analysed. Results showed that the H_2/CO ratio increased after employing biochar as catalyst when compared with steam reforming without biochar. Steam activation of biochar greatly improved its catalytic activities in reforming of light tar compounds. The yields of these light tar compounds, especially the non-oxygen-containing compounds, increased with increasing reforming time. The SSA, micro- and mesopore volumes in biochar raised during steam activation while stayed almost unchanged during tar reforming. The developed micro- and mesopores in biochar would enhance the diffusion of both small and large tar molecules into the internal surface of

biochar. The simultaneously generated O-containing functional groups during biochar activation are likely distributed in the newly created pores. Above all, it was found that the content of O-containing functional groups in biochar plays a more important role than the SSA and pore volume in determining its catalytic activity for tar reforming. Besides, the O-containing functional groups in biochar are likely to act as main active sites for the destruction of large aromatic ring systems and light non-oxygen-containing tar compounds. The O-containing functional groups enhance the breakdown of tar molecules to form tar radicals, promoting the rate of tar removal.

Acknowledgements

The authors acknowledge the support of the Australian Research Council (DP180101788, FT160100303). This project also received funding from the Australian Government through ARENA's Emerging Renewables Program. We wish to thank Richard Gunawan, Lei Zhang, Zhitao Wang, Li Dong, Yao Song and Shu Zhang for providing bio-oil and biochar samples. The SAXS measurement was conducted the SAXS/WAXS beamline at the Australian Synchrotron, part of ANSTO.

References

[1] Li C-Z. Special issue—gasification: a route to clean energy. Process Saf Environ Prot 2006;84:407–8.

[2] Sikarwar VS, Zhao M, Clough P, Yao J, Zhong X, Memon MZ, Shah N, Anthony EJ, Fennell PS. An overview of advances in biomass gasification. Energy Environ Sci

2016;9:2939–77.

[3] Vreugdenhil BJ, Zwart RWR. Tar formation in pyrolysis and gasification, report (ECN-E--08-087), Energy Research Centre of the Netherlands (ECN) 2009.

[4] Abdoulmoumine N, Adhikari S, Kulkarni A, Chattanathan S. A review on biomass gasification syngas cleanup. Appl Energy 2015;155:294–307.

[5] Guan G, Kaewpanha M, Hao X, Abudula A. Catalytic steam reforming of biomass tar: Prospects and challenges. Renew Sustain Energy Rev 2016;58:450–61.

[6] Song Y, Wang Y, Hu X, Hu S, Xiang J, Zhang L, Zhang S, Min Z, Li C-Z. Effects of volatile-char interactions on in situ destruction of nascent tar during the pyrolysis and gasification of biomass. Part I. Roles of nascent char. Fuel 2014;122:60–6.

[7] Ravenni G, Sárossy Z, Ahrenfeldt J, Henriksen UB. Activity of chars and activated carbons for removal and decomposition of tar model compounds – A review. Renew Sustain Energy Rev 2018;94:1044–56.

[8] Min Z, Yimsiri P, Asadullah M, Zhang S, Li C-Z. Catalytic reforming of tar during gasification. Part II. Char as a catalyst or as a catalyst support for tar reforming. Fuel 2011;90:2545–52.

[9] Abu El-Rub Z, Bramer EA, Brem G. Experimental comparison of biomass chars with other catalysts for tar reduction. Fuel 2008;87:2243–52.

[10] Hosokai S, Kumabe K, Ohshita M, Norinaga K, Li C-Z, Hayashi J-I. Mechanism of decomposition of aromatics over charcoal and necessary condition for maintaining its activity. Fuel 2008;87:2914–22.

[11] Buentello-Montoya DAA, Zhang X, Li J. The use of gasification solid products as catalysts for tar reforming. Renew Sustain Energy Rev 2019;107:399–412.

[12] Liu Y, Paskevicius M, Wang H, Fushimi C, Parkinson G, Li C-Z. Difference in tar reforming activities between biochar catalysts activated in H_2O and CO_2. Fuel 2020;271:117636.

[13] Liu Y, Paskevicius M, Wang H, Parkinson G, Veder JP, Hu X, Li C-Z. Role of O-containing functional groups in biochar during the catalytic steam reforming of tar using the biochar as a catalyst. Fuel 2019;253:441–8.

[14] Nestler F, Burhenne L, Amtenbrink MJ, Aicher T. Catalytic decomposition of biomass tars: The impact of wood char surface characteristics on the catalytic performance for naphthalene removal. Fuel Process Technol 2016;145:31–41.

[15] Zhang S, Song Y, Song YC, Yi Q, Dong L, Li TT, Zhang L, Feng J, Li WY, Li C-Z. An advanced biomass gasification technology with integrated catalytic hot gas cleaning. Part III: Effects of inorganic species in char on the reforming of tars from wood and agricultural wastes. Fuel 2016;183:177–84.

[16] Song Y, Wang Y, Hu X, Xiang J, Hu S, Mourant D, Li T, Wu L, Li C-Z. Effects of volatile-char interactions on in-situ destruction of nascent tar during the pyrolysis and gasification of biomass. Part II. Roles of steam. Fuel 2015;143:555–62.

[17] Song Y, Zhao Y, Hu X, Zhang L, Sun S, Li C-Z. Destruction of tar during volatile-char interactions at low temperature. Fuel Process Technol 2018;171:215–22.

[18] Buentello-Montoya D, Zhang X, Marques S, Geron M. Investigation of competitive tar reforming using activated char as catalyst. Energy Procedia 2019;158:828–35.

[19] Milne TA, Evans RJ, Abatzaglou N. Biomass gasifier “tars”: their nature, formation, and conversion. technical report (NREL/TP-570-25357). National Energy Laboratory. United States of America. 1998.

[20] Fuentes-Cano D, Gómez-Barea A, Nilsson S, Ollero P. Decomposition kinetics of model tar compounds over chars with different internal structure to model hot tar removal in biomass gasification. Chem Eng J 2013;228:1223–33.

[21] Hervy M, Weiss-Hortala E, Pham Minh D, Dib H, Villot A, Gérente C, Berhanu S, Chesnaud A, Thorel A, Le Coq L, Nzihou A. Reactivity and deactivation mechanisms of pyrolysis chars from bio-waste during catalytic cracking of tar. Appl Energy 2019;237:487–99.

[22] Zhang S, Asadullah M, Dong L, Tay HL, Li C-Z. An advanced biomass gasification technology with integrated catalytic hot gas cleaning. Part II: Tar reforming using char as a catalyst or as a catalyst support. Fuel 2013;112:646–53.

[23] Wu H, Quyn DM, Li C-Z. Volatilisation and catalytic effects of alkali and alkaline earth metallic species during the pyrolysis and gasification of Victorian brown coal. Part III. The importance of the interactions between volatiles and char at high temperature. Fuel 2002;81:1033–9.

[24] Min Z, Yimsiri P, Zhang S, Wang Y, Asadullah M, Li C-Z. Catalytic reforming of tar during gasification. Part III. Effects of feedstock on tar reforming using ilmenite as a catalyst. Fuel 2013;103:950–5.

[25] Min Z, Asadullah M, Yimsiri P, Zhang S, Wu H, Li C-Z. Catalytic reforming of tar during gasification. Part I. Steam reforming of biomass tar using ilmenite as a catalyst. Fuel

2011;90:1847–54.

[26] Jiang S, Hu X, Xia D, Li C-Z. Formation of aromatic ring structures during the thermal treatment of mallee wood cylinders at low temperature. Appl Energy 2016;183:542–51.

[27] Akhtar MA, Zhang S, Shao X, Dang H, Liu Y, Li T, Zhang L, Li C-Z. Kinetic compensation effects in the chemical reaction-controlled regime and mass transfer-controlled regime during the gasification of biochar in O_2. Fuel Process Technol 2018;181:25–32.

[28] Wang Y, Hu X, Mourant D, Song Y, Zhang L, Lievens C, Xiang J, Li C-Z. Evolution of aromatic structures during the reforming of bio-oil: Importance of the interactions among bio-oil components. Fuel 2013;111:805–12.

[29] Wang Y, Li X, Mourant D, Gunawan R, Zhang S, Li C-Z. Formation of aromatic structures during the pyrolysis of bio-oil. Energy and Fuels 2012;26:241–7.

[30] Kirby NM, Mudie ST, Hawley AM, Cookson DJ, Mertens HDT, Cowieson N, Samardzic-Boban V. A low-background-intensity focusing small-angle X-ray scattering undulator beamline. J Appl Crystallogr 2013;46:1670–80.

[31] Liu Y, Paskevicius M, Sofianos MV, Parkinson G, Li C-Z. In situ SAXS studies of the pore development in biochar during gasification. Carbon N Y 2021;172:454–62.

[32] Liu Y, Paskevicius M, Sofianos MV, Parkinson G, Wang S, Li C-Z. A SAXS study of the pore structure evolution in biochar during gasification in H_2O, CO_2 and H_2O/CO_2. Fuel 2021;292:120384.

[33] Dreiss CA, Jack KS, Parker AP. On the absolute calibration of bench-top small-angle X-ray scattering instruments: A comparison of different standard methods. J Appl

Crystallogr 2006;39:32–8.

[34] Spalla O, Lyonnard S, Testard F. Analysis of the small-angle intensity scattered by a porous and granular medium. J Appl Crystallogr 2003;36:338–47.

[35] Beaucage G. Approximations leading to a unified exponential power-law approach to small-angle scattering. J Appl Crystallogr 1995;28:717–28.

[36] Ilavsky J, Jemian PR. Irena : tool suite for modeling and analysis of small-angle scattering. J Appl Crystallogr 2009;42:347–53.

[37] Hu M, Laghari M, Cui B, Xiao B, Zhang B, Guo D. Catalytic cracking of biomass tar over char supported nickel catalyst. Energy 2018;145:228–37.

[38] Jess A. Mechanisms and kinetics of thermal reactions of aromatic hydrocarbons from pyrolysis of solid fuels. Fuel 1996;75:1441–8.

[39] J.M.Thomas, W.J.Thomas. Principles and Practice of Heterogeneous Catalysis. Second. Wiley-VCH.

[40] Coetzee GH, Sakurovs R, Neomagus HWJP, Morpeth L, Everson RC, Mathews JP, Bunt JR. Pore development during gasification of South African inertinite-rich chars evaluated using small angle X-ray scattering. Carbon N Y 2015;95:250–60.

[41] Hosokai S, Norinaga K, Kimura T, Nakano M, Li C-Z, Hayashi J-I. Reforming of volatiles from the biomass pyrolysis over charcoal in a sequence of coke deposition and steam gasification of coke. Energy and Fuels 2011;25:5387–93.

505

506

507

508

509

510